Behavior of steel frames with rotational friction dampers by endurance time method

Amir Shirkhani [a,b,*], Imad H. Mualla [c], Naser Shabakhty [b], Seyed Roohollah Mousavi [b]

[a] Department of Structural Engineering, Faculty of Civil Engineering, University of Tabriz, Tabriz, Iran
[b] Department of Civil Engineering, University of Sistan and Baluchestan, Zahedan, Iran
[c] CTO of DAMPTECH, Brovej B.118, Lyngby 2800, Denmark

ARTICLE INFO

ABSTRACT

Additional dampers are employed in order to decrease the dynamic response of structure against the earthquake and wind loading recently. Rotational friction damper (RFD) is one of them used in present study. The endurance time (ET) method is a new time-history-based dynamic pushover procedure in which structures are subjected to a gradually intensifying acceleration functions and their performance is judged based on the length of the time interval that they can satisfy required performance objectives. In this study, the application of ET method in nonlinear seismic analysis of steel frames equipped with the RFDs has been investigated. This method is used to calculate the optimum slip force of the RFD. The accuracy of ET method in predicting the response of structures in nonlinear analysis is investigated. Engineering demand parameters (EDPs) of frames with and without the RFDs such as displacement and maximum interstory drift ratio is estimated. Using ET curves, it is identified that the installation of the RFDs in underdesigned steel frames will decreases the maximum interstory drift ratio and will improves the seismic performance of such frames.

© 2015 Elsevier Ltd. All rights reserved.

1. Introduction

The performance of buildings can be increased employing additional dampers since these devices can absorb and damp some of the earthquake input energy [1]. Nowadays, friction dampers are used due to a high energy dissipation potential, low cost, easy installation and maintenance. Rotational friction damper (RFD) was introduced by Mualla. The primary experiments were done on a single story frame equipped with the RFD [2,3]. Nielsen and Mualla [4] concluded believes that damping system can be designed in such a way that has enough ability of energy dissipation in a structure under dynamic loading. Liao et al. [5] carried out a set of full-scale testing on shaking table. All the experiments revealed a proper performance of the RFD under seismic event. Kim et al. [6] used the friction damping system connected to a high strength tendon to increase the seismic capacity of existing structures. Komachi et al. [7] used the RFD to retrofit Ressalat jacket platform. The endurance time (ET) method is an analysis based on time history analysis that is going to predict engineering demand parameters (EDPs) of structures such as displacement and maximum interstory drift ratio in various intensity measures (IMs) under different dynamic excitations [8]. Since, up to now, there is not adequate investigation on the use of the ET method to calculate the optimum slip force of the

RFD and seismic analysis of steel frames with such damper, this method is examined and investigated in the present study. Since the common time history analysis requires a great deal of time to coordinate motions and there are a lot of analyses to be done, so ET method which is of vital importance in decreasing the numbers of analyses, it is created based on time history analysis. To be sure about the results according to ET method, a comparison is done between nonlinear time history (NTH) and ET results in this paper. In ET method, acceleration functions are made in such a way that linear and nonlinear response spectra intensified along with time as they are proportional to real earthquakes spectra average [9,10]. In addition to the investigation of the optimum slip force of the RFD, the maximum interstory drift ratio obtained by ET method is compared to NTH results in present research. The role of the RFD in the improvement of underdesigned steel frames using ET curves will be investigated too.

Notations	
BSE-1	Basic safety earthquake 1
BSE-2	Basic safety earthquake 2
CP	Collapse prevention
D_f	Displacement of structure equipped with the RFD
D_p	Displacement of structure without the RFD

* Corresponding author at: Department of Structural Engineering, Faculty of Civil Engineering, University of Tabriz, Tabriz, Iran. Tel.: +98 841 3354164.
E-mail addresses: shirkhani@tabrizu.ac.ir, shirkhani_amir@yahoo.com (A. Shirkhani).

E_h	Hysteric energy dissipated by the RFD
E_i	Input energy of structure equipped with the RFD
EDP	Engineering demand parameter
ET	Endurance time
F_a and F_v	Site coefficients
F_h	Slip force of the RFD
F_p	Prestress force to prevent the brace bars from buckling
F_s	Equivalent yield strength
F_y	Yield stress
$f(\tau)$	Response history
h_a	Height of the RFD
IDA	Incremental dynamic analysis
IM	Intensity measure
INBC	Iranian National Building Code
K_{bd}	Stiffness of the damping system
K_f	Lateral stiffness of the primary frame
K_p	Post-yield stiffness
K_t	Initial elastic stiffness
LS	Life safety
MCE	Maximum considered earthquake
M_f	Rotational friction strength (slip frictional moment) of the RFD
M_u	Torque demand imposed by the earthquake on the RFD if it is locked
NTH	Nonlinear time history
PBEE	Performance-based earthquake engineering
PGA	Peak ground acceleration
R_d	Displacement reduction factor
R_e	Remaining energy factor
R_f	Base shear reduction factor
RFD	Rotational friction damper
S_1	Long-period response acceleration parameter
S_a	Acceleration response spectrum
SPI	Seismic performance index
S_s	Short-period response acceleration parameter
T_i	Fundamental period of the frame
t_{Target}	Target time used for optimization procedure (= 10 s in this study)
u_A	Displacement of frame with the RFD
u_{A0}	Displacement amplitude
V_f	Base shear of structure equipped with the RFD
V_p	Base shear of structure without the RFD
η_{lM}	Normalized RFD strength
Ω	Max_Abs operator
θ	Rotation of the RFD

2. Rotational friction damper (RFD)

The RFD is included vertical plates, horizontal plates and friction pad discs placed between steel plates [11]. This damper is presented in Fig. 1. The vertical plates are connected to the beam center to have a free movement and efficient energy dissipation. The horizontal plates are connected to the inverted V-brace at the end points. The bracing
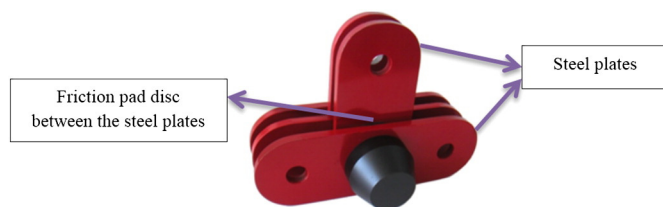

Fig. 1. The RFD [12].

can be presented in order to prevent their sudden buckling. The bracing bars are connected to columns as a pin in order to provide a free movement for damper [2].

Fig. 2 shows a single story frame equipped with the RFD. When a lateral force excites a frame structure, the beam tends to move horizontally. The bracing system and the friction forces developed at the interface of the steel plates and friction pads will resist the horizontal motion [2]. Frictional hinge is shown in the figure.

3. The basic model description and behavior of the RFD

The basic model under consideration consists of a single story moment-resisting primary frame and a damping system with two components, the RFD itself and the supporting bracing members as shown in Fig. 2. A possible approach to modeling is the bilinear-hysteresis representation. The bilinear force-displacement relationship stems from the action in parallel of rigid-plastic RFD and perfectly elastic primary frame and braces. The equivalent yield strength F_s, initial elastic stiffness K_t and post-yield stiffness K_p are defined as follows:

$$F_s = \left(\frac{M_f}{h_a}\right) / \left(\frac{K_t}{K_{bd}}\right) \tag{1}$$

$$K_t = K_f + K_{bd} \tag{2}$$

$$K_p = K_f \tag{3}$$

where h_a is the height of the RFD. M_f is the frictional moment. K_f and K_{bd} are the lateral stiffness of the primary frame and the stiffness of the damping system, respectively [2]. Typically the mass of the damping system is small compared with the mass of the frame and typically the elastic deformations in the damping system are small compared with the deformations from sliding in the frictional hinge of the damping system. Then it is relevant—as done here—to consider the case, where the mass and the elastic deformations of the damping system are neglected. Now the lateral force F_h in the damping system in point A, see Fig. 2, and the work conjugated displacement u_A can characterize the state in the frictional hinge [4] as shown on Fig. 3(a). In the figure, u_{A0} is the displacement amplitude. The energy dissipated by the RFD per loading cycle is equivalent to the area enclosed in the moment–rotation curve [6], as shown in Fig. 3(b). The figure shows the behavior of the RFD.

3.1. Verification of model

To investigate the accuracy of the basic model in this paper, the displacement results for a single story frame under Elcentro earthquake excitation are compared with the results by Mualla and Belev [2]. Bracing bars connected the damper with two types of pretensioned force (F_p), one $0.2F_p$ and other one equal to F_p are considered. The results obtained by Mualla and Belev and the response of that structure in the present study are presented in Fig. 4(a) and (b) respectively.

4. The concept of the endurance time method

In the ET method, structures are subjected to a predesigned intensifying acceleration function and their performance is recognized based on the time interval during which they can satisfy predefined performance criteria [13]. Acceleration function is a predesigned excitation in endurance time, different from the real ground motions. ET acceleration function intensity will increased along with time. The time duration from the start of the excitation the limit point considering an EDP of interest is called the endurance time with respect to that EDP. Since the intensity of the excitation is increasing with time, a longer endurance time means that the structure has been subjected to a higher equivalent intensity before the intended
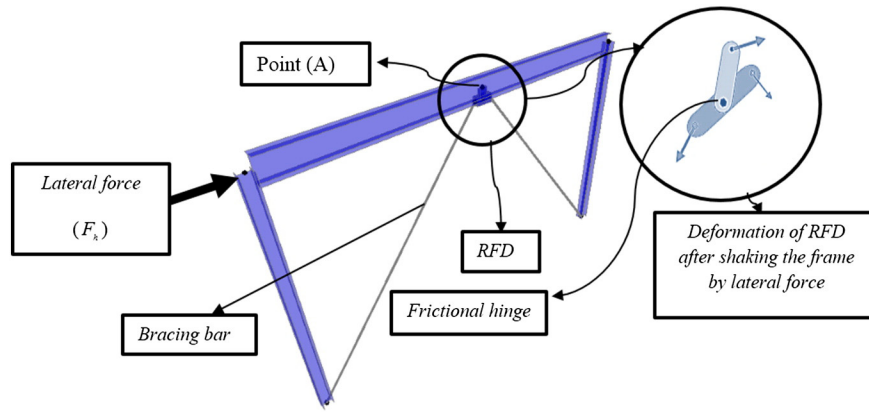
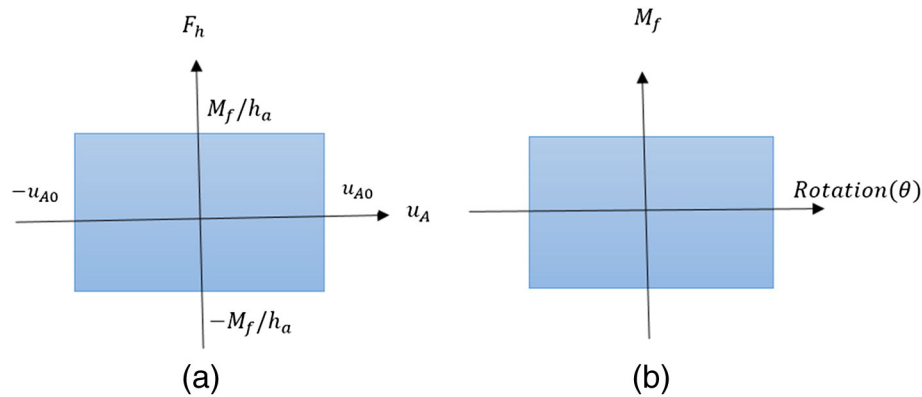**Fig. 2.** Single story frame equipped with the RFD.

Fig. 3. Frictional damping system behavior: (a) force displacement, (b) moment rotation.

EDP exceeds its maximum limit value [14]. If the main characteristics of the earth movements assembled by ET acceleration function, the real response of structures will be assessed properly according the performance-based earthquake engineering (PBEE) [15]. In PBEE, the structures are designed in such a way that can experience various building performance objectives at different seismic hazard levels. Each specified time is related to a specified IM. Hence, in ET analysis, the equivalent times of IMs are used instead of different IMs representing different levels of excitation. A schematic representation of ET analysis for three prototype structures is shown in Fig. 5. These structures are subjected to an ET acceleration function, and their performances are recorded through the analysis using a time history analysis procedure. Because of the increasing trend of the applied acceleration function, structures gradually go through the elastic phase to yielding and nonlinear inelastic phases. Based on the structure characteristics, they present different responses at different levels of excitations. Eventually, all of them experience global dynamic instability and will collapse under the intensifying excitation that is being applied [16].

One of the purpose of the present research is the verification of ET method using a comparison between the results this method and NTH. Hence, the three acceleration functions applied in this research (ETA20f01-3) presented in Fig. 6 are created in this way as their response spectra remain proportional to that of the average of seven real ground motions spectra [17]. Time duration of the acceleration functions is 20.48 s. The ground motions are selected among the used records in FEMA440 [18] which are recorded on soil type C [14,19,20]. The average response spectrum is smoothed and used for generation of the ETA20f set. The specifications of this set of ground motions are presented in Table 1. The response spectrum of any window of the
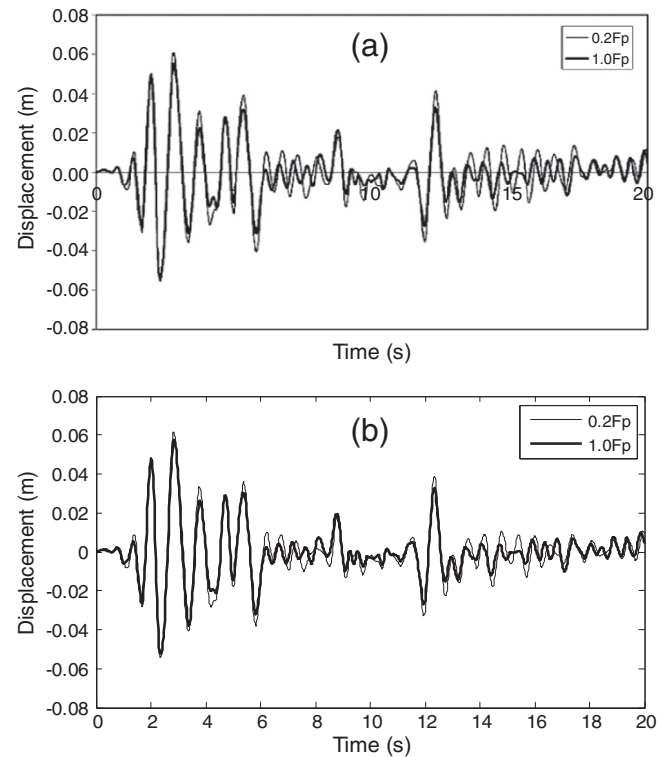

Fig. 4. Displacement response: (a) results by Mualla and Belev [2], (b) results of this study.
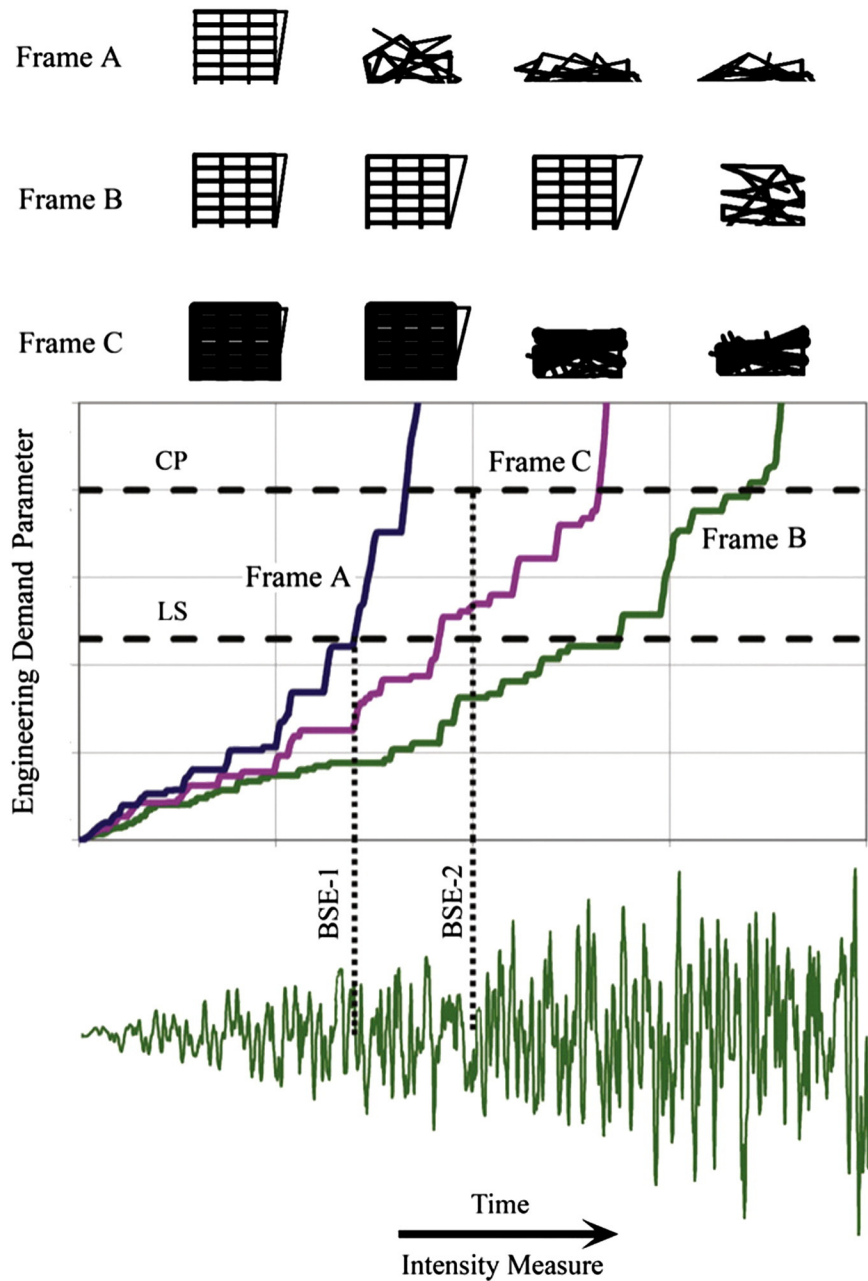
Fig. 5. Schematic representation of ET analysis and its application in PBEE [16].

ETA20f set of acceleration functions from $t_0 = 0$ to $t_1 = t$ resembles that of the average response spectrum of the seven ground motions with a scale factor that is proportional with time (t) [14]. This scale factor is equal to 1.0 for $t_{Target} = 10$ s in present study.

The general response of spectrum of ASCE/SEI 41-06 [21], namely, BSE-2 earthquake hazard level, is used in present research, with the following characteristics: $S_s = 1.5$, $S_1 = 0.6$, $F_a = 1.0$ and $F_v = 1.3$; [14].

The comparison of average of acceleration response spectra of ETA20f set in various times with the average of response spectra of seven records multiplied at equivalent scale factors is displayed on Fig. 7. As it be can be seen, the response spectrum of each time window in acceleration functions of endurance time from $t_0 = 0$ to $t_1 = 10$ s is matched with the average response spectrum of seven ground motions. It be noted that in each time, response spectra of ET are remained consistent with the spectra average of seven scaled records. For example, it is 0.5, 1.5, 2 times the average spectra of seven scaled records are at $t = 5$ s, $t = 15$ s and $t = 20$ s, respectively [16].

5. Specifications of steel frames

To make a comparison between the seismic performance of steel moment frames with and without the RFDs, two-dimensional frames with 3, 7 and 12 stories that have three bays are considered in present study. These frames are designed in two groups: the first group is designed based on Iranian Standard No. 2800 [22] and Iranian National Building Code (INBC) section 10 [23], which are close to AISC ASD design code [24] for steel structures [16]. The names of these frames end with the letter S. The soil is type II of Iranian Standard No. 2800 in the current study which is matched with soil type C of Standard ASCE/SEI 41-06. The horizontal component of ground motions is used for dynamic analysis [16]. In nonlinear analysis, these frames are placed on BSE-2 earthquake hazard level of Standard ASCE/SEI 41-06, equal to PGA = 0.6 g, while they are designed for an area with a high relational hazard, to Iranian Standard No. 2800, equal to PGA = 0.35 g. Hence, a comparison is made between seismic behavior of frames with and without the
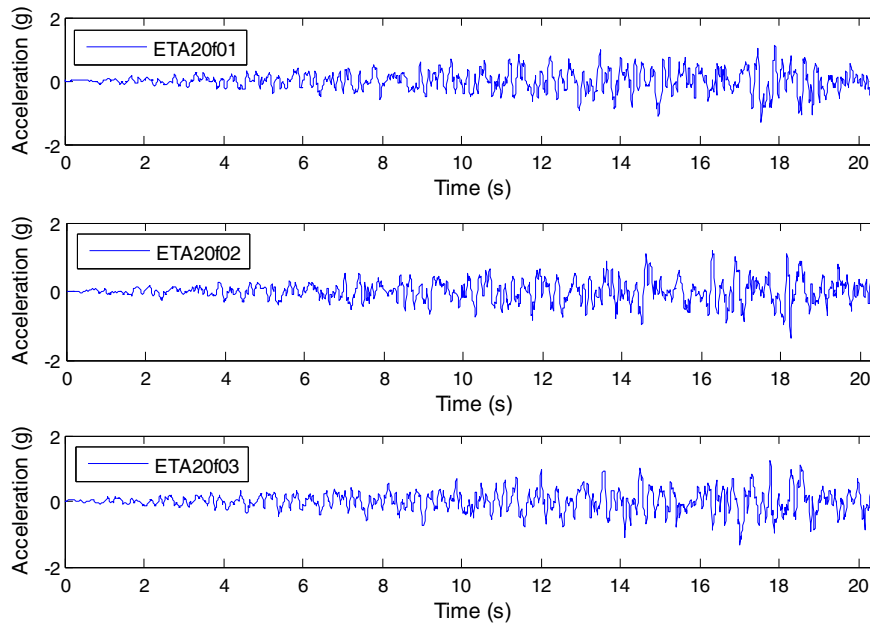
Fig. 6. Acceleration functions of ETA20f set used in this study.

Table 1
Ground motions set used in this study [19].

Date	Earthquake name	Magnitude (Ms)	Station number	Component (deg)	PGA (g)	Abbreviation
06/28/92	Landers	7.5	12 149	0	0.171	LADSP000
10/17/89	Loma Prieta	7.1	58 065	0	0.512	LPSTG000
10/17/89	Loma Prieta	7.1	47 006	67	0.357	LPGIL067
10/17/89	Loma Prieta	7.1	58 135	360	0.450	LPLOB000
10/17/89	Loma Prieta	7.1	1 652	270	0.244	LPAND270
04/24/84	Morgan Hill	6.1	57 383	90	0.292	MHG06090
01/17/94	Northridge	6.8	24 278	360	0.514	NRORR360

RFDs. The second group is underdesigned frames that they have been designed based on one half of the codified base shear. The names of these frames end with the letter W. In the naming of frames, prefixes "Mf" and "RFDf" represent moment frames without and with the RFD, respectively. The schematic of frames is presented in Fig. 8. The designed sections for Mf03S frame, the specifications of frames in the present study and the period of free vibration of frames with and without the RFDs are presented in Tables 2–4, respectively.
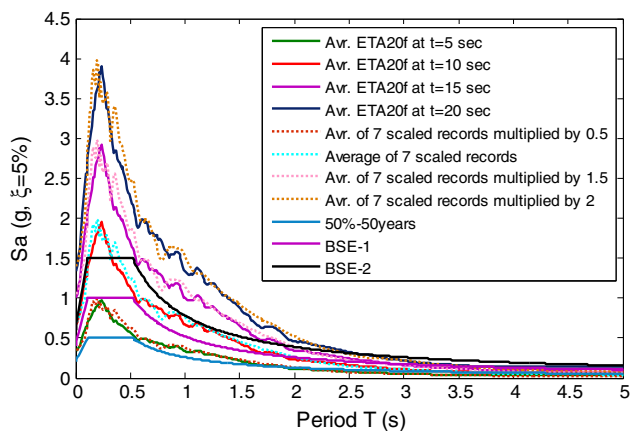

Fig. 7. Consistency of average of acceleration response spectra of ETA20f set in different time with average of response spectra of seven scaled records.
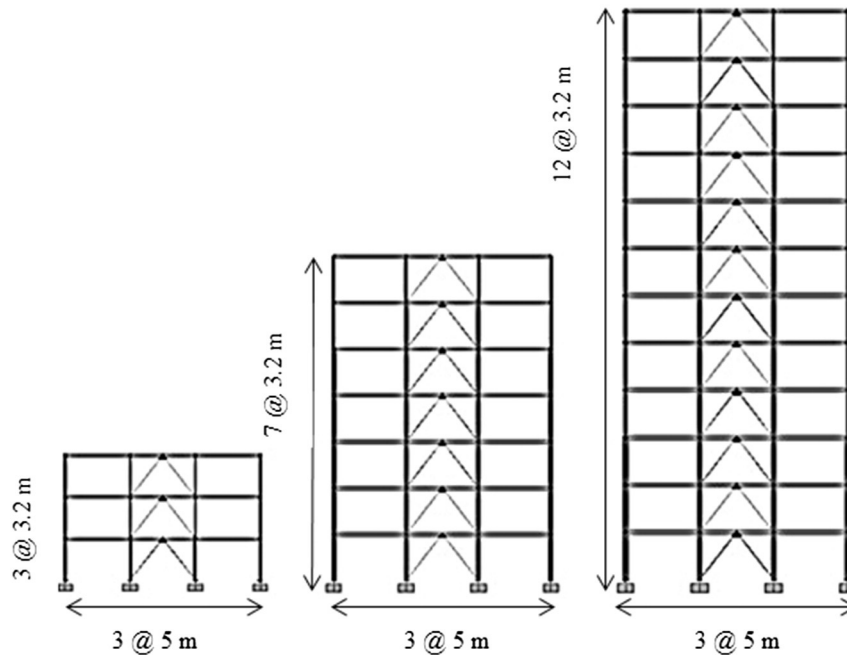
It is obvious that, by adding the RFDs to the structure, the free vibration will be reduced and as a result stiffness increases. It is explicit that underdesigned frames have a larger free vibration and a lower stiffness compared to the standard designed frames.

6. Seismic analysis

6.1. Scaling of seven records

To be consistent with ASCE/SEI 41-06, the seven records are scaled such a way that the average of the ordinates of the 5% damped linear response spectra does not fall below the design spectrum for the period range $0.2T_i$–$1.5T_i$, where T_i is the fundamental period of vibration of each frame. The records are scaled individually rather than scaling them as pairs since the analyzed structures are two dimensional [14,16]. The scale factors of frames with and without the RFDs for NTH analysis are shown in Table 5.

6.2. Equivalent time of ET functions

To determine the equivalent time of ET acceleration functions, the spectrum used for producing them must be scaled for each frame in the period range $0.2T_i$ to $1.5T_i$. The scaling method is similar to the one used for scaling seven records. The scale factors calculated for each frame are multiplied by 10 to obtain the equivalent time of the frames. The constant 10 is used since the response spectrum of ET acceleration function in $t_{Target} = 10$ s is matched with the average of ground motions spectrum with a unit scale factor [14]. Equivalent times of ET

Fig. 8. Schematic of the frames with the RFDs.

acceleration functions for frames employed in present study are shown in Table 6.

6.3. Seismic performance index (SPI) of the RFD

To investigate the seismic performance of steel moment frames with the RFDs, the diameter of bracing bar equal to 35 mm with $F_y = 355$ MPa, where F_y is yield stress. The RFDs are considered as central form with $h_a = 0.2$ m, where h_a is height of the RFD, since the central damping system has the maximum dissipation of energy [5]. Seismic analysis is carried out on these frames under seven records and ETA20f set. Time steps are considered as 0.02 s in all analyses. To obtain the optimum slip force of the RFD, SPI must be calculated. This index introduced by Mualla and Belev is [2] is estimated by Eq. (4):

$$SPI = \sqrt{R_d^2 + R_f^2 + R_e^2} \tag{4}$$

in which R_d, R_f and R_e represent displacement reduction factor, base shear reduction factor and remaining energy factor, respectively [2]:

$$R_d = \frac{D_f}{D_p} \tag{5}$$

Table 4
Period of free vibration of the frames with the RFDs (RFDf) and without the RFDs (MF).

Frames	Period of free vibration (s)
Mf03S	0.945
RFDf03S	0.477
Mf07S	1.422
RFDf07S	0.953
Mf12S	2.018
RFDf12S	1.539
Mf03 W	1.170
RFDf03W	0.500
Mf07 W	1.563
RFDf07 W	1.000
Mf12W	2.165
RFDf12W	1.608

Table 2
Designed sections for Mf03S frame.

Story level	Beam	Column
1	HE260A	Tubo240X240X17.5
2	HE260A	Tubo200X200X17.5
3	HE220A	Tubo180X180X12.5

Table 3
Specifications of the frames.

Frames	Number of Stories	Weight (KN)	Design base shear (KN)
MF03S	3	1458.06	182.27
MF03W	3	1452.57	90.74
MF07S	7	3491.58	312.84
MF07 W	7	3473.52	155.59
MF12S	12	6065.42	414.86
MF12W	12	6031.58	206.30

Table 5
The final scale factors of all ground motions employed in NTH analysis for frames with and without the RFDs.

Frames	LADSP 000	LPAND 270	MHG 06090	LPGIL 067	LPLOB 000	LPSTG 000	NRORR 360
Mf03S	3.98	2.98	1.75	2.62	2.73	1.85	1.09
RFDf03S	3.87	2.49	2.22	2.14	2.11	2.02	1.32
Mf07S	4.20	3.13	2.05	2.83	3.74	1.66	1.13
RFDf07S	3.98	2.99	1.75	2.62	2.74	1.84	1.09
Mf12S	4.78	3.65	2.78	3.47	5.46	1.71	1.31
RFDf12S	4.33	3.27	2.20	2.94	4.08	1.65	1.15
Mf03 W	4.08	3.01	1.82	2.67	3.11	1.74	1.10
RFDf03 W	3.89	2.52	2.19	2.21	2.27	2.02	1.31
Mf07 W	4.34	3.29	2.23	2.96	4.11	1.65	1.15
RFDf07 W	3.99	3.02	1.75	2.63	2.83	1.82	1.08
Mf12W	4.92	3.75	2.93	3.64	5.85	1.73	1.37
RFDf12W	4.39	3.34	2.29	3.00	4.22	1.65	1.16

Table 6
Equivalent times of ETA20f set for the frames with and without the RFDs.

Frames	Equivalent time (s)
Mf03S	11.1
RFDf03S	10.9
Mf07S	12.3
RFDf07S	11.1
Mf12S	14.2
RFDf12S	12.7
Mf03 W	11.5
RFDf03 W	11.0
Mf07 W	12.7
RFDf07 W	11.2
Mf12W	16.9
RFDf12W	12.9

Table 7
Optimum slip force of the RFD.

	RFDF 03S	RFDF 03 W	RFDF 07S	RFDF 07 W	RFDF 12S	RFDF 12W
Optimum slip force (w)	0.076w	0.085w	0.059w	0.053w	0.030w	0.033w

$$R_f = \frac{V_f}{V_p} \tag{6}$$

$$R_e = (E_i - E_h)/E_i \tag{7}$$

where D_f is the displacement of structure equipped with the RFD, D_p is the displacement of structure without the RFD, V_f is the base shear of structure equipped with the RFD, V_p is base shear of structure without the RFD, E_i is the input energy of structure equipped with the RFD and E_h is hysteric energy dissipated by the RFD [2]. The normalized RFD strength is defined by the ratio:

$$\eta_M = M_f/M_u \tag{8}$$

in which M_f is rotational friction strength (slip frictional moment) of the RFD and M_u is torque demand imposed by the earthquake on the RFD if it is locked and does not slide during the excitation. To obtain the optimum slip force of the RFD, the normalized RFD strength η_M from 0 to 1 is increased in 20 steps with 0.05 increments. The SPI calculated for seven ground motions and three ETA20f acceleration functions. After calculation the results mean in each step for seven ground motions and three

acceleration functions separately, the minimum value of SPI is determined and then the corresponding normalized RFD strength of each of them is multiplied at the respective mean M_u in order to calculate the optimum slip frictional moment. The optimum slip force of the RFD is obtained by the division of the optimum slip frictional moment on the height of the RFD ($h_a = 0.2$ m). Note that $\eta_M = 0$ (if the slip force of the RFD is equal to 0 without energy dissipation) is consistent with unbraced primary frame and $\eta_M = 1$ (if the slip force of the RFD will be high and it doesn't running) consistent with braced frame by the locked RFD [2].

The SPI diagram of the RFD for NTH and ET results mean are presented in Fig. 9.

As can be seen in Fig. 9, the minimum values of SPI for the NTH and ET results mean of three stories frame are 0.98 and 0.83, respectively. These values are 0.99 and 0.96 for 7 stories frame and 1.10 and 1.07 for 12 stories frame, respectively. Therefore, it can be concluded that the minimum values of SPI for NTH and ET results mean will by increased by increasing the number of stories. The minimum value of SPI for NTH and ET analyses is occurred in $\eta_M = 0.15$ and $\eta_M = 0.1$ respectively for these 7 and 12 stories frames. The difference of the least value in ET and NTH results mean is about 3% in both of them. It is concluded that there will be a higher consistency between the diagrams of damper seismic performance index according to NTH and ET results mean by increasing the number of frames stories. NTH and ET results mean, ET analysis can be used instead of NTH analysis to decrease the large number of nonlinear analyses to obtain the optimum slip force. Therefore, the optimum slip force of the RFD in terms of the frame weight is represented in Table 7. In which, w is the weight of each frame.
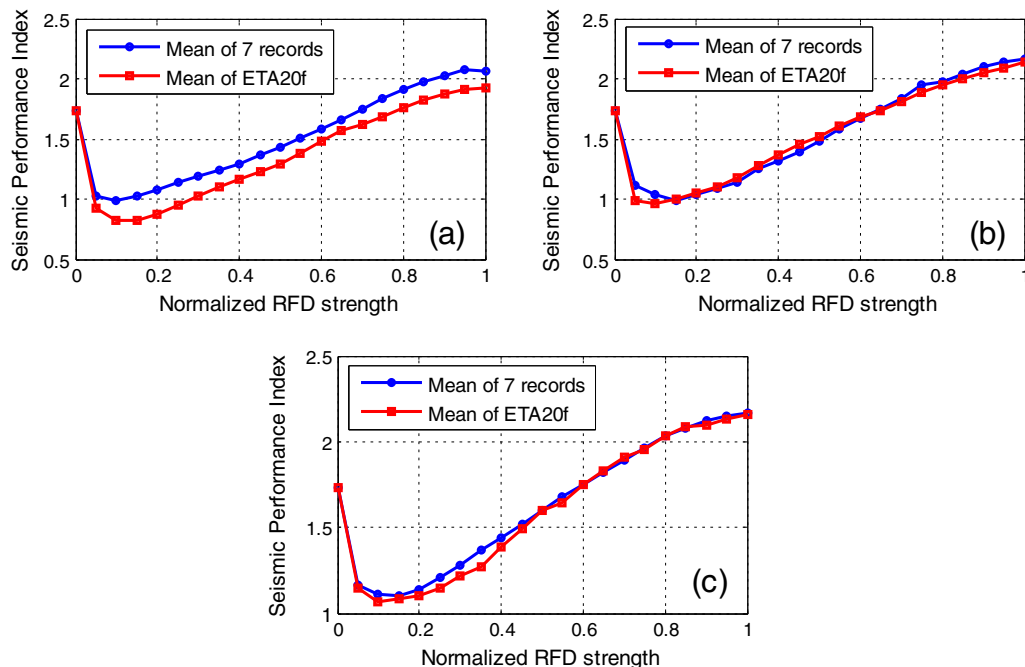
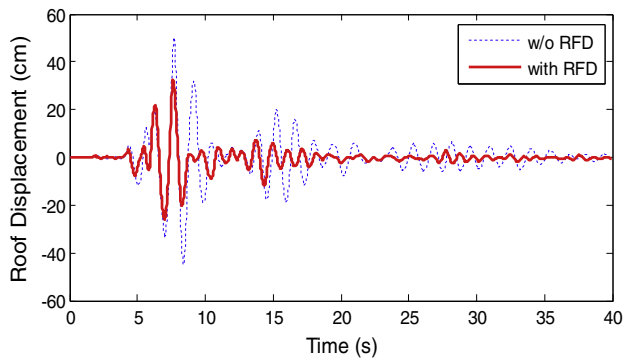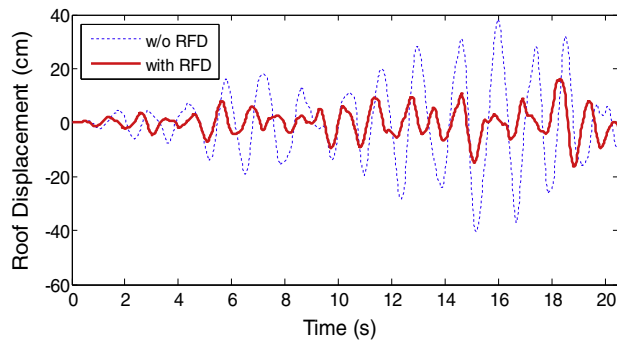**Fig. 9.** SPI of the RFD for frames: (a) RFDf03S; (b) RFDf07S; (c) RFDf12S.

Fig. 10. Comparison between roof displacement of Mf07S and RFDf07S frames under LPSTG000.

Fig. 13. Maximum interstory drift ratio of RFDf07S frame at different story levels obtained by NTH analysis.

6.4. NTH and ET results

In this study, interesting EDPs such as maximum roof displacements and maximum interstory drift ratio of frames with and without the RFDs are investigated. A comparison of the roof displacement is made between Mf07S and RFDf07S frames under LPSTG000 record (Fig. 10). According to the roof displacement history of these frames, it is determined that by adding the RFDs to Mf07S frame, the maximum roof displacement will be decreased by 34.69%. This amount is 59.66% for ETA20f02 (Fig. 11).

The present research aim at studying a comparison of the maximum interstory drift ratio results analyzed by NTH with ET method to investigate the ET results accuracy. Figs. 12 and 13 show the maximum interstory drift ratios of Mf07S and RFDf07S frames at different story levels obtained by NTH analysis, respectively.

Fig. 12 reveals that the greatest value of maximum interstory drift ratio is predicted in sixth story by LPSTG000 record. The mean of seven ground motions results predicts this value in the sixth story, too. According to Fig. 13, it is observed that the diagram of maximum interstory drift ratio for RFD07S frame compared with Mf07S frame has more regular results. It obvious that LPSTG000 record predicts the greatest value of maximum interstory drift ratio in the 2nd story which is the greatest value among the results of seven ground motions. The mean of seven ground motions results predicts the greatest value of maximum interstory drift ratio in the 2nd story. Figs. 14 and 15 show the maximum interstory drift ratios of Mf07S and RFDf07S frames obtained by ET analysis, respectively.

Fig. 11. Comparison between roof displacement of Mf07S and RFDf07S frames under ETA20f02.

Fig. 14. Maximum interstory drift ratio of Mf07S frame at different story levels obtained by ET analysis.
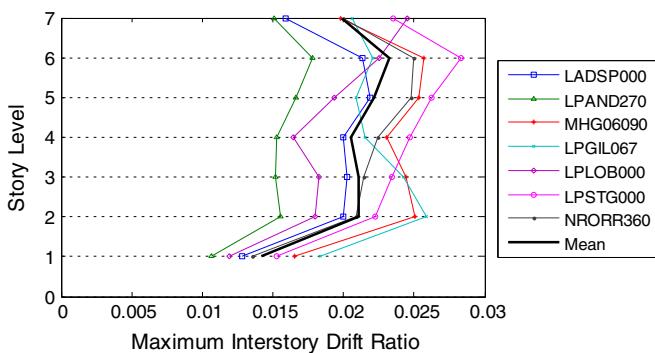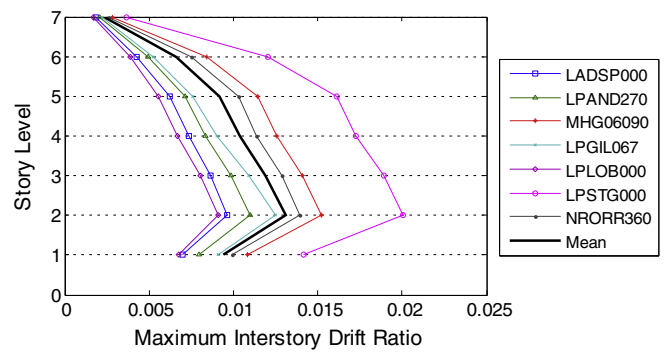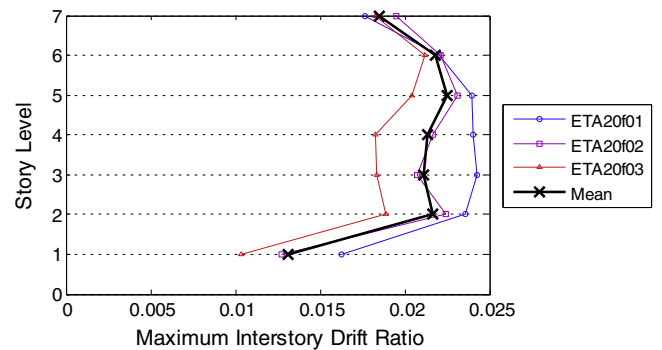

Fig. 12. Maximum interstory drift ratio of Mf07S frame at different story levels obtained by NTH analysis.
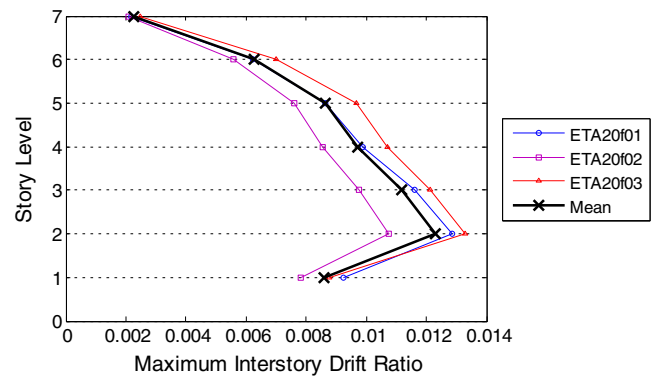

Fig. 15. Maximum interstory drift ratio of RFDf07S frame at different story levels obtained by ET analysis.
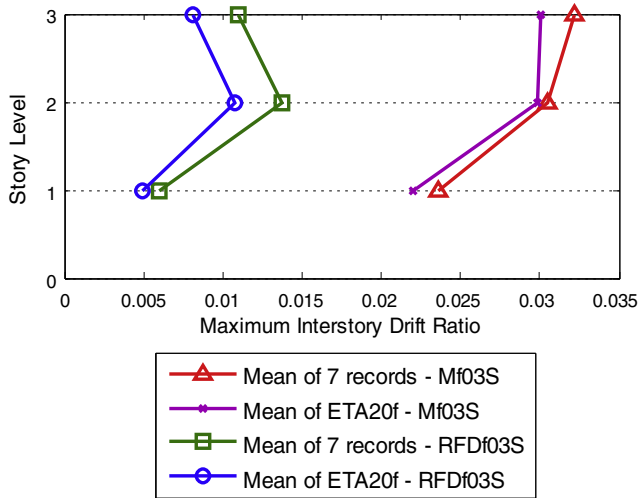
Fig. 16. Comparison of maximum interstory drift ratio between Mf03S and RFDf03S frames at different story levels obtained by NTH and ET analyses.

According to Fig. 14, it is identified that ETA20f01 acceleration function predicts the maximum interstory drift ratio in 3th story but ETA20f02 and ETA20f03 functions predict it in 5th and 6th story respectively. The ET analysis results mean predicts it in 5th story. As it is presented in Fig. 15, three acceleration functions employed in this study and their mean predict the maximum interstory drift ratio in 2nd story. There is a comparison of maximum interstory drift ratio diagrams of Mf03S and RFDf03S frames by NTH and ET analyses in Fig. 16. The figure shows that by installing the RFDs in Mf03S frame, the maximum interstory drift ratios decrease strongly. Fig. 17 represents this comparison according to Mf03W and RFDf03W frames. As it is obvious the maximum value of such diagrams, are greater than that of diagrams in Fig. 16, since these frames are underdesigned compared to the pervious analyzed frames.

There is a comparison of maximum interstory drift ratio diagrams of Mf07S and RFDf07S frames by NTH and ET analyses in Fig. 18. It is obvious that by adding the RFDs to the structure, the maximum interstory drift ratios decrease strongly, so there will be more arrangement in NTH analysis results mean with ET results mean. There is a little difference between NTH and ET results mean. The difference is about 0.0007 for maximum value of two analysis method. Hence, according to all results, the accuracy of ET method results will be proved.
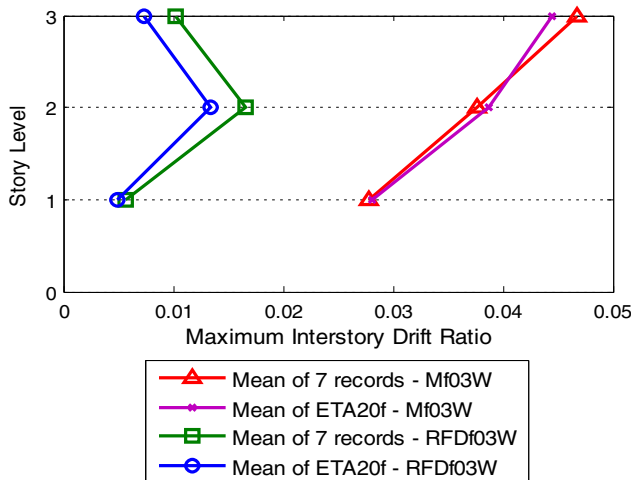

Fig. 17. Comparison of maximum interstory drift ratio between Mf03W and RFDf03W frames at different story levels obtained by NTH and ET analyses.
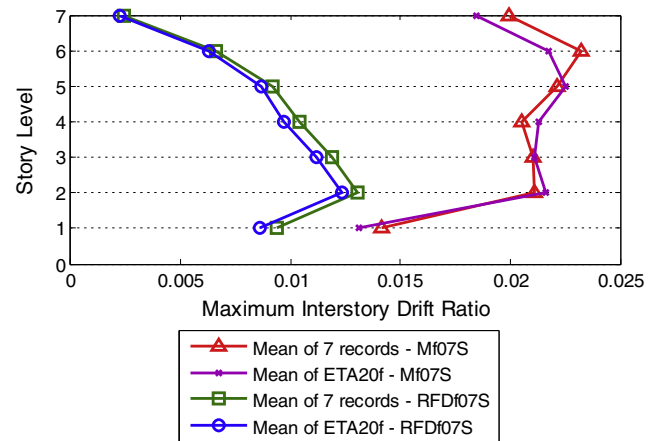

Fig. 18. Comparison of maximum interstory drift ratio between Mf07S and RFDf07S frames at different story levels obtained by NTH and ET analyses.

Fig. 19 represents this comparison according to Mf07W and RFDf07W frames. Fig. 20 shows this comparison for Mf12S and RFDf12S frames and Fig. 21 shows it for Mf12 W and RFDf12 W frames.

6.5. ET curve

ET analysis results usually are presented by increasing ET curve, where y coordinate at each time value, t, corresponds to the maximum absolute value of required EDP in the time interval [0, t] presented in Eq. (9).

$$\Omega\ (f(t)) \equiv \mathrm{Max}(\mathrm{Abs}(f(\tau) : \tau \in [0, t])). \tag{9}$$

In equation Ω is the Max_Abs operator on $f(t)$, which is a desired response history such as base shear, interstory drift ratio, damage index and other parameters are of interest. The x coordinate axis of an ET curve is time correlated with IM. It is of a high value to note that the arrangement of the coordinate axes of an ET curve is in a reversed place compare ET with standard push over and IDA curves. ET curves are usually serrated since the statistical specifications and dispersion of ET analysis results are in the nonlinear range. The response value sometimes does not pass the maximum value experienced before in a time interval. Hence, the obtained curve possesses a constant value in that interval. Moving average procedure is employed to solve this problem in order to decrease the serrated nature of ET curves. First, the ET curves of three acceleration functions are averaged, and then moving average method is used [16]. Fig. 22 presents the drawing process of ET maximum interstory drift ratio curves of the ETA20f set for Mf03W frame.
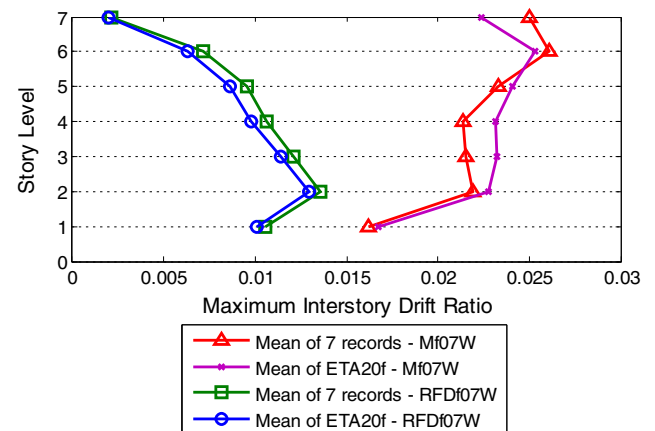

Fig. 19. Comparison of maximum interstory drift ratio between Mf07 W and RFDf07 W frames at different story levels obtained by NTH and ET analyses.
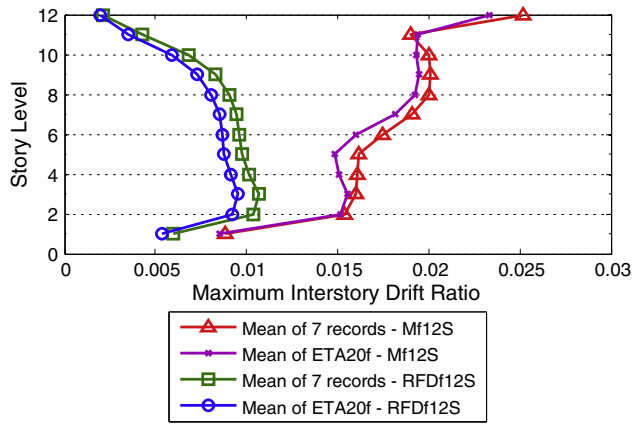
Fig. 20. Comparison of maximum interstory drift ratio between Mf12S and RFDf12S frames at different story levels obtained by NTH and ET analyses.

Fig. 22. ET maximum interstory drift ratio curves of the ETA20f set for Mf03 W frame.

Fig. 23 shows the ET maximum interstory drift ratio curves of the ETA20f set for Mf03W and RFDf03W frames. The results of the ET analysis are obtained until the equivalent time calculated for these frames [16]. Underdesigned frames are used due to representation of the effects of the RFD on their seismic performance improvement. As it is obvious from Fig. 23, the maximum interstory drift ratio is equal to 0.02417 in equivalent time 11.5 s for Mf03W frame, but it is equal to 0.004508 in equivalent time 11 s for RFDf03W frame, which it reveals the seismic performance of the Mf03W frame is improved by adding the RFDs. A typical ET curve introduces very important information about performance of structure in different IMs. The behavior of structure in low IMs is linearly until it reaches a certain point at which the first plastic hinge is created. As the intensity of acceleration function increasing along with time, the structures experience some kinds of deformations which lead to collapse limit. Collapse does not occur for the frames of Fig. 23 before t = 20 s, but the structure can reach to collapse level by generating ET acceleration functions with a longer duration. Mentioned figure reveal that how ET analysis can recognize the performance of structure in different IMs.

As it is presented in Fig. 23, Mf03W frame which is without the RFDs has a weak performance, but by adding the RFDs to it (RFDf03W), its performance will get better efficiently. Maximum interstory drift ratios obtained at the equivalent times are also presented in the figure. According to the performance objectives defined for the design or rehabilitation of the frames, it can be checked whether these frames satisfy such objectives or not. For instance, if the basic safety objective will be selected for these frames, the collapse prevention (CP) building
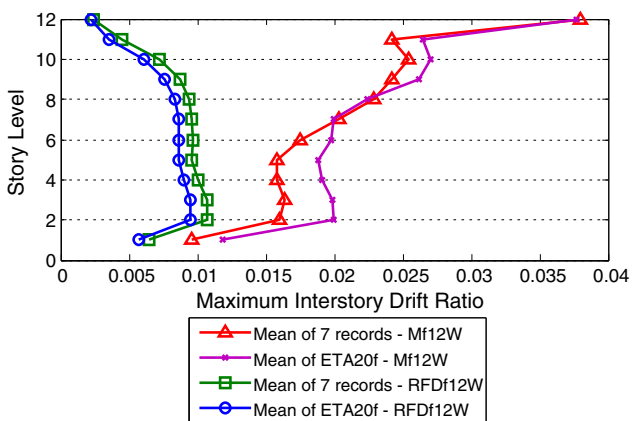
performance level should be achieved for the MCE (the same BSE-2) hazard level. There for the response spectrum employed for calculating equivalent times in this study reveals MCE hazard level, the drift ratio must be less than 5% according to ASCE/SEI 41-06. The maximum interstory drift ratios of frames are less than 5% which is presented in Fig. 23. To check the frames for life safety (LS) building performance, appropriate response spectra (for instance BSE-1 earthquake hazard level) should be employed for calculating the equivalent time. Then the response of frames should be compared to the desired values [16]. Therefore by using ET curve, it can be shown that the performance of underdesigned steel frames will be improved by adding the RFDs which leads to decreasing the maximum interstory drift ratio proportional with the equivalent times of the frames.

6.6. The hysteresis cycle for the RFD

The hysteresis cycles for the RFD in 3th story of RFDf07S frame under NRORR360 record and ETA20f01 are presented in Fig. 24. As it is obvious, there is an appropriate correspondence between the hysteresis cycles and the behavior of the RFD which is mentioned before. As expected, the RFD shows stable hysteretic behavior and dissipate large amount of seismic energy.

7. Summary and conclusions

Endurance time (ET) method is a new dynamic analysis procedure that aims at estimating seismic performance of structures by subjecting them to predesigned intensifying acceleration functions. However,

Fig. 21. Comparison of maximum interstory drift ratio between Mf12W and RFDf12W frames at different story levels obtained by NTH and ET analyses.
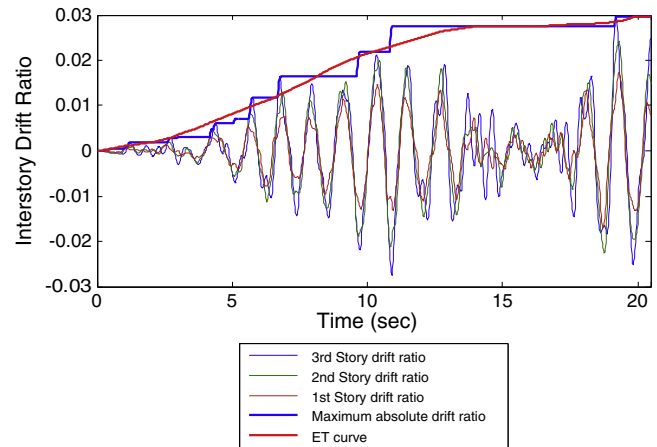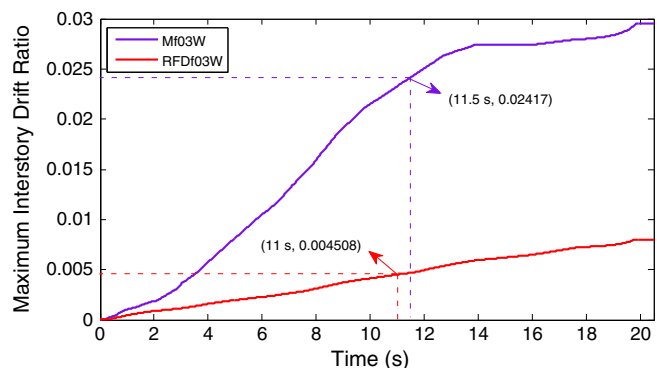

Fig. 23. ET maximum interstory drift ratio curves of the ETA20f set for Mf03 W and RFDf03W and values of equivalent time of the time history analysis.
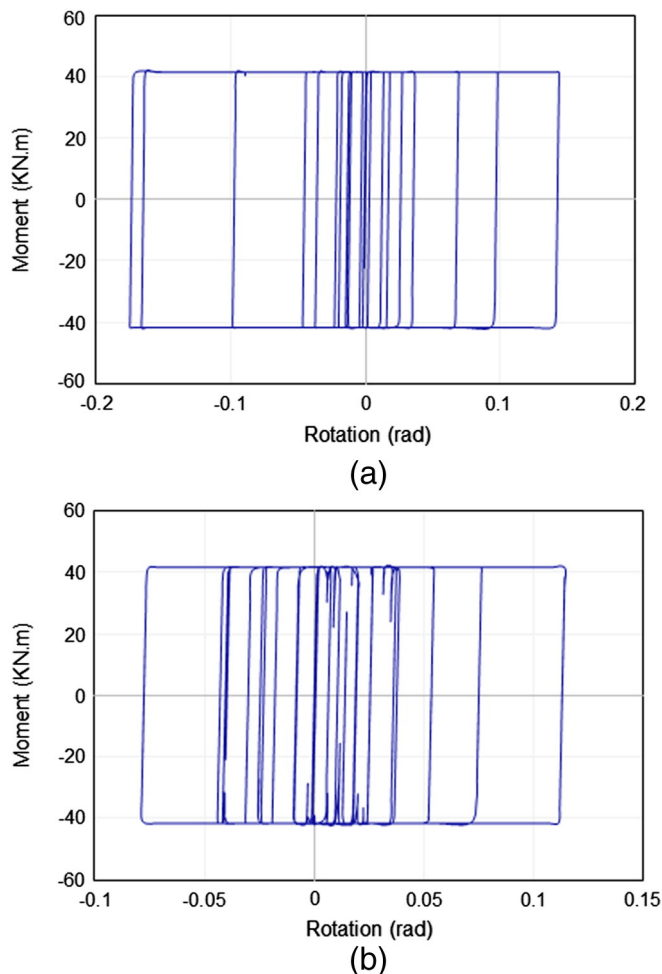
Fig. 24. Behavior of the RFD in 3th story of RFDf07S frame under excitation: (a) NRORR360 record; (b) under ETA20f01.

since, up to now, there was not adequate investigation on the use of the ET method to calculate the optimum slip force of the RFD and the evaluation of the effects of the RFDs on steel frames, this method has been examined and investigated in this paper. New findings of this study are listed below:

- The minimum value of SPI for NTH and ET results mean is increased along with increasing the number of frame stories.
- There was a higher consistency between the SPI diagrams obtained from NTH and ET results mean.
- According to the differences of the minimum values of SPI and the optimum slip force of the RFD in each earthquake record and each acceleration function, to be sure about the RFD proper performance in the next earthquakes, the results mean of seven records or that of three acceleration functions should be considered.
- Due to the proximity and consistency of SPI of the RFD obtained from NTH and ET results mean; 57% of dynamic nonlinear analyses have been decreased by employing ET instead of NTH analysis to achieve the optimum slip force of the RFD.
- The optimum slip force of the RFD (with respect to the frames weight) will be decreased by increasing the number of frame stories.
- The maximum interstory drift ratio diagrams obtained from seven ground motions get more arrangement compared to each other by adding the RFDs to the structure. This event has been occurred for the maximum interstory drift ratio diagrams obtained from three ET acceleration functions too.

- The maximum interstory drift ratios decrease severely by adding the RFDs to the structure which leads to more arrangement between NTH and ET analyses results.
- There was a little difference between maximum interstory drift ratio diagrams of NTH and ET analyses results. Hence, according to all of the results, the accuracy of ET method is proved.
- Using the ET curve, it has been concluded that by adding the RFDs to the underdesigned steel frames, their seismic performance will be improved properly and the maximum interstory drift ratio will be decreased proportional with the equivalent times of the frames.
- The stable hysteretic behavior of the RFD represents that its suitable performance in energy dissipation.

Appendix A. Supplementary data

Supplementary data to this article can be found online at http://dx.doi.org/10.1016/j.jcsr.2015.01.016.

References

[1] Ghasemi M. The Friction pendulum Bracing. (in Persian) [dissertation] Tehran: Sharif University of Technology; 2006.
[2] Mualla IH, Bellev B. Performance of steel frames with a new friction damper device under earthquake excitation. Eng Struct 2002;24:365–71.
[3] Mualla IH. Experimental evaluation of new friction damper device, 12WCEE, no 1048 ; 2000.
[4] Mualla IH, Nielsen L. A Friction Damping System Low Order Behavior and Design. Department of Civil Engineering DTU-bygning; 2002, R-0302002.
[5] Liao W, Mualla IH, Loh C. Shaking table test of a friction damped frame structure. Struct Des Tall Special Build 2004;13:45–54.
[6] Kim J, Choi H, Min KW. Use of rotational friction dampers to enhance seismic and progressive collapse resisting capacity of structures. Struct Des Tall Special Build 2011;20:515–37.
[7] Komachi Y, Tabeshpour MR, Golafshani AA, Mualla IH. Retrofit of Ressalat jacket platform (Persian Gulf) using friction damper device. J Zhejiang Univ Sci A Appl Phys Eng 2011;12:680–91.
[8] Estekanchi HE, Vafai A, Sadeghazar M. Endurance time method for seismic analysis and design of structures. Sci Iran 2004;11:361–70.
[9] Riahi HT, Estekanchi HE, Seyedain Boroujeni S. Application of endurance time method in nonlinear seismic analysis of steel frames. Procedia Eng 2011;14: 3237–44.
[10] Shirkhani A, Shabakhty N, Mousavi SR, Esmaeilpour Javadi E. Assessment of seismic performance of steel moment frames retrofitting with X-brace by ET method. (in Persian), 4th National conference on earthquake and structure, Kerman, Iran; 2013.
[11] Mualla IH, Nielsen L. Parameters influencing the behavior of a new friction damper device. Papers in Structural Engineering and Materials. Technical University of Denmark; 2000. p. 49–58.
[12] Mualla IH, Jakupsson ED. A rotational friction damping system for buildings and structures. Proc Dan Soc Struct Sci Eng 2010;98(3):47–98.
[13] Estekanchi HE, Riahi HT, Vafai A. Endurance time method: a dynamic pushover procedure for seismic evaluation of structures. First European Conference on Earthquake Engineering and Seismology, Geneva, Switzerland, 3-8 September; 2006.
[14] Estekanchi HE, Riahi HT, Vafai A. Application of endurance time method in seismic assessment of steel frames. Eng Struct 2011;33:2535–46.
[15] Riahi HT, Estekanchi HE. Application of endurance time method for estimating maximum deformation demands of structures. First European Conference on Earthquake Engineering and Seismology, Geneva, Switzerland; 2006.
[16] Riahi HT, Estekanchi HE. Seismic assessment of steel frames with the endurance time method. J Constr Steel Res 2010;66:780–92.
[17] Estekanchi HE, Vafai A, Riahi HT. Endurance time method: from ideation to application. PEER 2009/02. Berkeley: University of California; 2009.
[18] FEMA. Improvement of Nonlinear Static Seismic Analysis Procedures. FEMA-440 Washington (DC): Federal Emergency Management Agency; 2005.
[19] Bazmuneh A, Estekanchi HE. Application of endurance time method in performance based design: buckling-restrained braced frame. (in Persian) Islam Azad Univ J Civ Eng 2010;2(1):10–25.

[20] Basim MCh, Estekanchi HE. Application of endurance time method in optimal design of viscous dampers in performance based design of steel frames. (in Persian), 5th National congress on civil engineering, Mashhad, Iran; 2010.

[21] ASCE standard ASCE/SEI 41-06. Seismic Rehabilitation of Existing Buildings. American Society of Civil Engineers; 2007.

[22] BHRC. Iranian Code of Practice for Seismic Resistant Design of Buildings. standard no. 2800-05. 3rd ed. Tehran: Building and Housing Research Center; 2005.

[23] Office of collection and extension of national building code. section 10: Design and construction of steel structures, 4th ed. Tehran; 2005.

[24] American Institute of Steel Construction. Allowable Stress Design Manual of Steel Construction. 9th ed. Chicago: AISC; 1989.